This article has been accepted for publication in a future issue of this journal, but has not been fully edited. Content may change prior to final publication. Citation information: DOI 10.1109/TSG.2018.2829438, IEEE Transactions on Smart Grid

# Survivability of Autonomous Microgrid during Overload Events

Wei Du, *Member, IEEE,* Robert H. Lasseter, *Life Fellow, IEEE,* Amrit S. Khalsa, *Senior Member, IEEE*

***Abstract*—Grid-forming sources are voltage sources that draw necessary currents to meet any load changes. A load step can cause part or all of these sources to become overloaded in a microgrid. This paper presents an overload mitigation controller that addresses the two overload issues in a microgrid by actively controlling the sources' frequency. When part of the sources in a microgrid is overloaded, the controller autonomously transfers the extra load to other sources by rapidly reducing its frequency. The frequency difference between sources during transient results in a change of phase angle, which redistributes the power flow. When all sources in a microgrid are overloaded, each source keeps dropping the frequency. Therefore, under frequency load shedding can be used to trip the non-critical loads resulting in the survival of microgrid. The advantages of these concepts are that communications between sources are not needed during transient, and the robust voltage control is maintained. Simulation and field tests from CERTS/AEP microgrid test site verify that the control strategy is effective in both purely inverter-based microgrids and inverter & generator mixed microgrids.**

***Index terms*—microgrid, survivability, overload mitigation, grid-forming source, droop control.**

## I. INTRODUCTION

The microgrid is a cluster of Distributed Energy Resources (DERs) and loads with the ability to operate in both islanded mode and grid-connected mode, and to isolate itself from the grid seamlessly with little or no disruption to the loads [1]. The microgrid concept was first defined and demonstrated by the Consortium for Electric Reliability Technology Solutions (CERTS) [1-3], and receives wide attention in recent years [4-9].

The grid-forming sources are crucial to microgrid operation due to their roles in voltage and frequency regulation. These sources are fundamentally voltage sources and draw the necessary currents to meet any load changes. When some sources are dispatched near their maximum generation in an islanded microgrid, a load step can cause these sources to become overloaded. The most severe contingency is in islanded mode with more loads than sources, all sources become overloaded. An overload may collapse the dc bus voltage of a grid-forming inverter [10], stall a synchronous generator [11], or even collapse the entire microgrid. Up to now there are not many references studying the overload issues of microgrids. It was once thought that an inner current loop could effectively limit the over-currents of grid-forming sources, but reference [12] points out that the use of reference saturation of inner current loop causes instability. Some references switch control modes between grid-forming control and grid-following control [13-15]. The grid-forming sources can be switched to grid-following control mode when their ratings are exceeded. However, the modes switching method only works when part of the sources are overloaded. When all the grid-forming sources in an islanded microgrid are overloaded, the switching from grid-forming control to grid-following control directly collapses the microgrid. There is no control of the microgrid's voltage or frequency. The virtual impedance concept has been used to limit the fault currents in a microgrid [16, 17]. However, the overload issue is different from the fault issue because there is no significant voltage drop during overload. The use of a virtual impedance during overload may result in a significant voltage drop, which deteriorates power quality. Reference [10] designed a control strategy for a single stage grid-forming PV inverter, which prevents its dc bus voltage from collapsing due to an increase in load. Reference [11] proposed a maximum torque controller for a synchronous generator, which prevents it from stalling in a microgrid. However, references [10] and [11] only studied the case when part of the sources in a microgrid is overloaded, but the case when all sources become overloaded is not studied. A central controller based on a fast communication network can trip the non-critical loads easily when all sources are overloaded, but this approach reduces reliability because communication failure may collapse the microgrid.

This paper presents an overload mitigation controller that addresses the two overload issues by actively controlling the sources' frequency. When part of the sources in a microgrid is overloaded, the controller autonomously transfers the extra load of the overloaded source to other sources by reducing its frequency rapidly. The frequency difference between sources during transient results in a change of phase angle, which redistributes the power flow. When all sources in a microgrid are overloaded, each grid-forming source keeps dropping the frequency, so the under frequency load shedding can be used to trip the non-critical loads, which allows microgrid to survive. The advantages of these concepts are that communications between sources are not needed, and the robust voltage control is maintained. Finally, simulation and field test results from CERTS/American Electric Power (AEP) microgrid test site verify that this strategy is effective in both purely inverter-based microgrids and inverter & generator mixed microgrids.

Wei Du is currently with the Pacific Northwest National Laboratory, Richland, WA 99352 USA (e-mail: wei.du@pnnl.gov). He was with the University of Wisconsin-Madison while working on this research.

Robert H Lasseter is with the Department of Electrical and Computer Engineering, University of Wisconsin-Madison, Madison, WI 53706-1691 USA (e-mail: Lasseter@engr.wisc.edu).

A. S. Khalsa is with the American Electric Power, Groveport, OH 43125 USA (e-mail: askhalsa@aep.com)

This article has been accepted for publication in a future issue of this journal, but has not been fully edited. Content may change prior to final publication. Citation information: DOI 10.1109/TSG.2018.2829438, IEEE Transactions on Smart Grid

## II. DROOP-CONTROLLED, GRID-FORMING SOURCE

### A. Grid-Forming Source

A grid-forming source is intrinsically a voltage source behind a coupling reactance $X_L$, which regulates both voltage and frequency of the microgrid. The basic model is shown in Fig. 1.

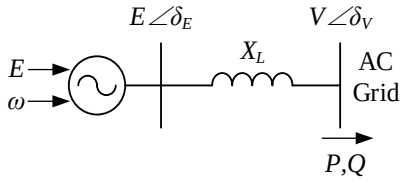


Fig. 1 A grid-forming source.

$$\delta_p = \delta_E - \delta_V \tag{1}$$

$$P = \frac{EV}{X_L}\sin\delta_p \approx \frac{EV}{X_L}\delta_p \tag{2}$$

$$Q = \frac{E^2 - EV\cos\delta_p}{X_L} \approx \frac{E(E-V)}{X_L} \tag{3}$$

The coupling reactance $X_L$ plays a critical role in controlling the P and Q injected into the microgrid. If $X_L$ is properly designed, according to equations (1) to (3), P is approximately linear with phase angle $\delta_p$, and Q is approximately linear with internal voltage magnitude E. Therefore, the P vs. f droop control and Q vs. V droop control can be applied on grid-forming source, Fig. 2 [18]. An inappropriate $X_L$ deteriorates the droop control effects. $X_L$ cannot be too large, or P will no longer be linear with $\delta_p$. $X_L$ cannot be too small, or the line resistance R has to be considered in Fig. 1. The value of $X_L$ can be between 5% and 15%, which usually guarantees the effectiveness of droop control.

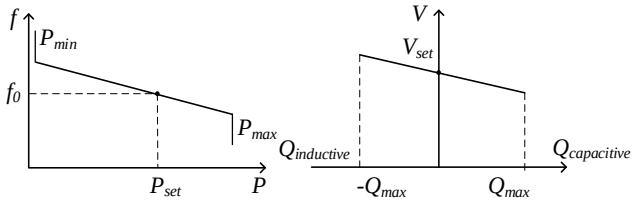


Fig. 2 P vs. f droop and Q vs. V droop.

### B. CERTS Droop Controls

Fig. 3 shows the control configuration of CERTS droop controls [18]. The inverter is connected to the microgrid through an LC filter and an additional inductance. The grid side real power, reactive power, and voltage magnitude are calculated and passed through a first order low pass filter to obtain the filtered P, Q, and $V_{mag}$. Then the P vs. f droop controller adjusts the frequency ω of the inverter internal voltage, where $m_p$ is the P vs. f droop gain, $\omega_0$ is the rated grid frequency, and $P_{set}$ is the power set point. The Q vs. V droop controller regulates the inverter internal voltage magnitude E through a PI controller, where $m_q$ is the Q vs. V droop gain, and $V_{set}$ is the voltage set point. $k_{pv}$ and $k_{iv}$ are the proportional and integral gains of the PI controller, respectively. With E and ω obtained, the PWM signals can be generated. The CERTS droop controls enable multiple grid-forming sources to work together in a microgrid. It is important to point out that both $L_1$ and $L_2$ in Fig. 3 should be counted for the coupling reactance $X_L$ in Fig. 1 when CERTS droop controls are used.

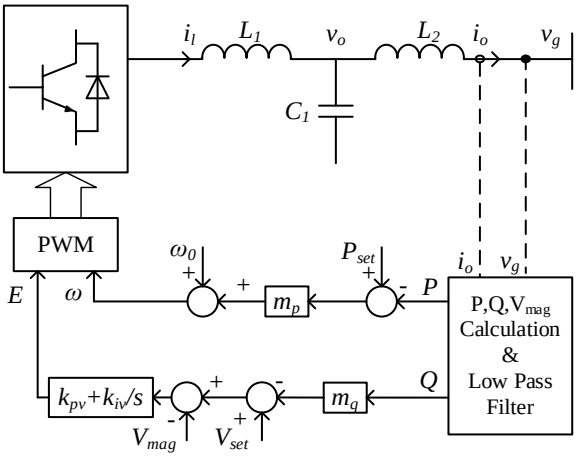


Fig. 3 CERTS Droop Control.

## III. OVERLOAD ISSUE & SOLUTION

Voltage sources autonomously track loads. The major down side is that sources can become overloaded. There are two overload issues when using grid-forming inverters: a. One or more of the sources are overloaded. b. All the sources are overloaded. This section presents an overload mitigation controller that handles both overload issues by actively controlling the source's frequency. When some but not all of the sources in a microgrid are overloaded, the controller reduces the frequency of the overloaded source faster than other sources', which results in a frequency difference between sources. This frequency difference during transient reduces the phase angle of the overloaded source relative to other sources, so its output power could be mitigated. The extra loads of the overloaded source are transferred to other sources which are not in overload. When all the sources are overloaded, frequency continues to drop activating under frequency load shedding. Fig. 4 shows the proposed overload mitigation controller. It is a PI controller added to the P vs. f droop control, where $k_{ppmax}$ and $k_{ipmax}$ are the proportional gain and integral gain, respectively. Noted that there is a zero upper/lower limiter in this controller, which indicates that the controller will only be activated when P exceeds $P_{max}$ or when P is below $P_{min}$.

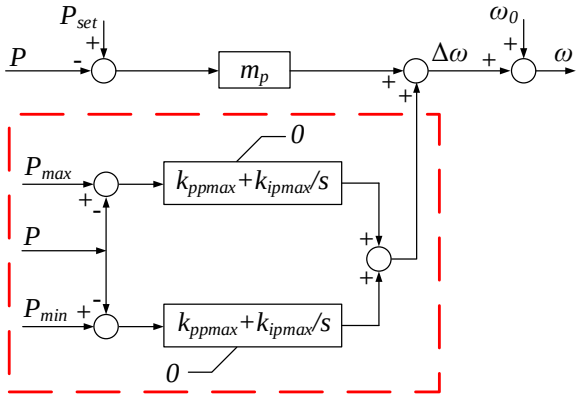


Fig. 4 Overload mitigation controller.

This article has been accepted for publication in a future issue of this journal, but has not been fully edited. Content may change prior to final publication. Citation information: DOI 10.1109/TSG.2018.2829438, IEEE Transactions on Smart Grid

## A. Overload Transfer

Sources should be dispatchable in a microgrid, this is realized by changing the set point $P_{set}$ of P vs. f droop curve, Fig. 2. Therefore, the Energy Management System (EMS) can change power flow between sources by adjusting sources' set points. Sometimes some sources may be dispatched near their maximum ratings, a load step may cause these sources to become overloaded. Fig. 5 and Fig. 6 demonstrate this issue. Consider a two-source system as shown in Fig. 5, each source has a 60 kW rated capacity. A1 is dispatched at 55 kW and A2 is dispatched at 5 kW. When a 30 kW Load 2 is switched on, both A1 and A2 increase their output currents instantaneously to meet this extra load, Fig. 6. It can be seen in Fig. 6 that the load step results in the overload of A1.

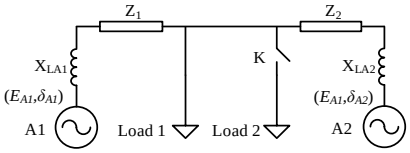


Fig. 5 A two-source system.

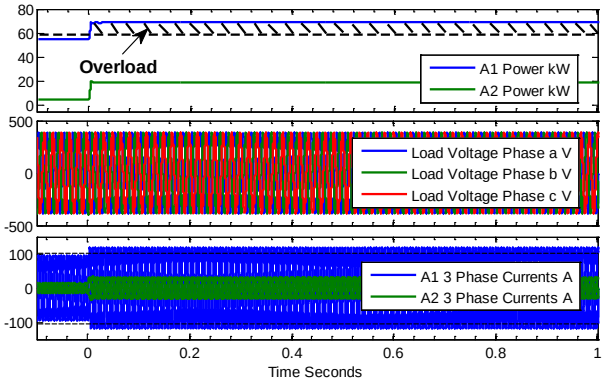


Fig. 6 Demonstration of partial overload issue.

Although A1 becomes overloaded, A2 still has sufficient capability to relieve the overload. With the proposed overload mitigation controller, once the output power P of A1 exceeds its maximum $P_{max}$, the controller reduces its frequency rapidly. By reducing A1's frequency faster than A2's frequency during transient, the phase angle of A1 relative to A2 is reduced, which redistributes the power flow between A1 and A2. Therefore, the extra load of A1 can be autonomously transferred to A2. Fig. 7 shows the field test results of overload transfer [2]. It can be seen that the overload of A1 is mitigated in about 0.2 s. Fig. 8 (a) and (b) further demonstrate this partial overload issue and overload mitigation on P vs. f droop curves, respectively. It can be seen that with conventional droop control the output power of A1 exceeds its maximum rating, while with the overload mitigation controller the P vs. f droop curve becomes vertical when the maximum rating is reached.

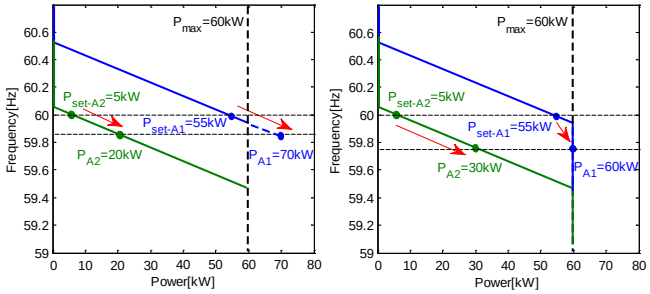


(a) (b)

Fig. 8 Demonstration of (a) partial overload issue and (b) overload mitigation on P vs. f droop curves.

A full-order small signal model of the two-source system is established to study how the parameters influence the stability [19]. The initial equilibrium state is that A1's overload mitigation controller is activated and A2 works in a normal droop control mode. It is found that two key parameters are important for the small signal stability: the coupling reactance $X_L$ and the proportional gain $k_{ppmax}$. Fig. 9 (a) and (b) show the traces of eigenvalues as the $k_{ppmax}$ and $X_L$ change, respectively. Fig. 9 (a) shows the trace of eigenvalues as $k_{ppmax}$ increases from 1 rad/s to 120 rad/s, where $X_L$ = 0.12 pu. The system is

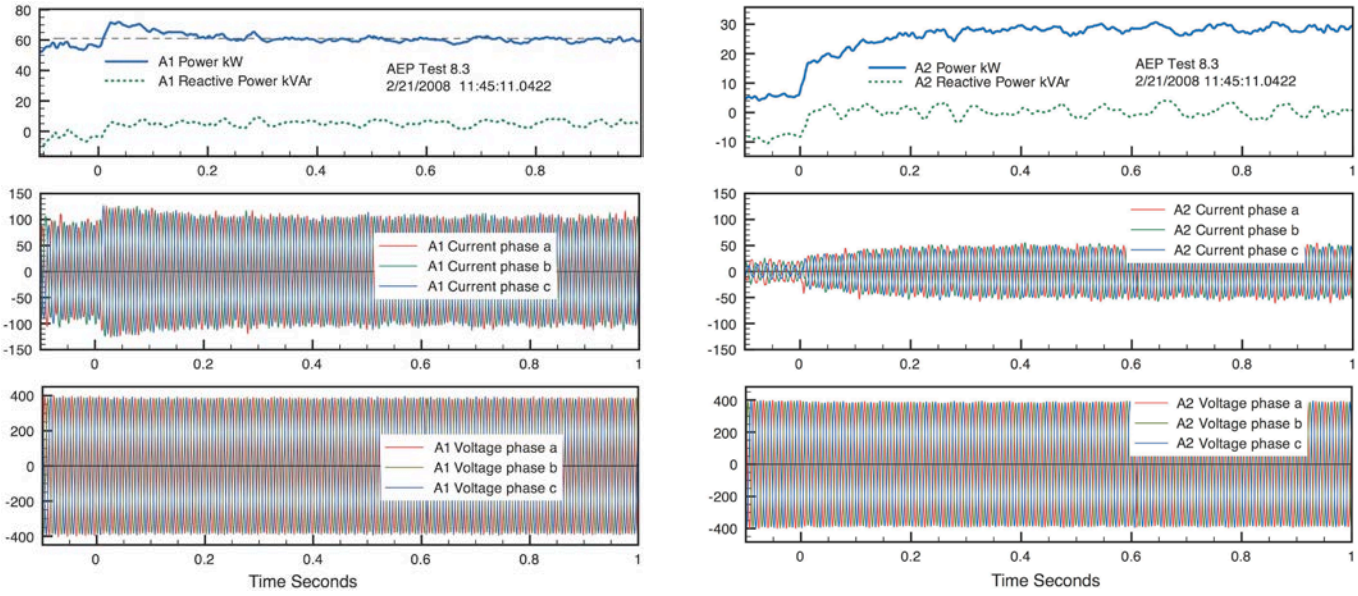


(a) (b)

Fig. 7 Field Test Results of Overload Transfer. (a) Responses of A1. (b) Responses of A2.

This article has been accepted for publication in a future issue of this journal, but has not been fully edited. Content may change prior to final publication. Citation information: DOI 10.1109/TSG.2018.2829438, IEEE Transactions on Smart Grid

less damped with the increase of $k_{ppmax}$. When $k_{ppmax}$ is greater than 95 rad/s, the system becomes unstable. Fig. 9 (b) shows the trace of eigenvalues as $X_L$ increases from 0.02 pu to 0.14 pu, where $k_{ppmax}$= 3 rad/s.

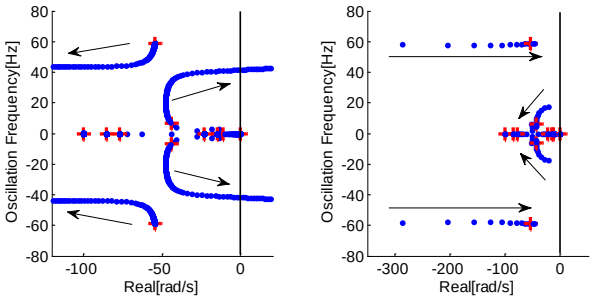


Fig. 9 Traces of eigenvalues when (a) $k_{ppmax}$ increases from 1 rad/s to 120 rad/s, where $X_L$=0.12 pu and (b) $X_L$ increases from 0.02 pu to 0.14 pu, where $k_{ppmax}$=3 rad/s.

Furthermore, an approximately linear stability boundary is obtained through a $k_{ppmax}$ vs. $X_L$ two dimensional eigenvalue scan, Fig. 10 [20]. It shows that a larger $X_L$ allows a larger $k_{ppmax}$ to maintain the stability, which indicates a well-designed coupling reactance $X_L$ is very important for the robustness of droop control, as mentioned in Section II A. When designing the controller parameter $k_{ppmax}$, both the dynamic response and stability should be considered. A larger $k_{ppmax}$ can mitigate the overload faster, but the stability might be affected if $k_{ppmax}$ is too large. Therefore, there is a trade-off between the dynamic response and stability when selecting $k_{ppmax}$. The red '+' icons in Fig. 9(a), (b), and Fig. 10 represent the parameters used in the field test of Fig. 7. It can be seen that the field test selects a very conservative gain of $k_{ppmax}$.

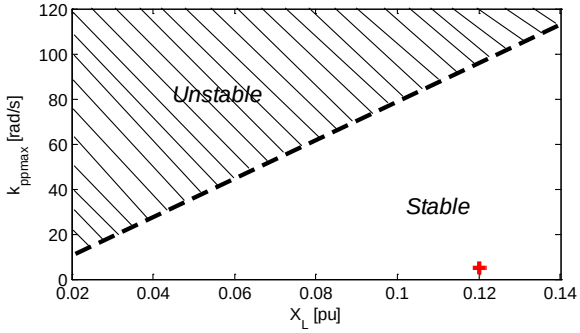


Fig. 10 Small signal stability boudary.

## B. Under Frequency Load Shedding

In some more severe circumstances such as loss of generation in an islanded microgrid or when a grid-connected microgrid goes into islanded mode with more loads than sources, the whole microgrid can become overloaded. Since all the sources are overloaded, one natural way is to trip some non-critical loads. With the proposed overload mitigation controller, the frequency of each grid-forming source continues dropping during overload. Therefore, the traditional under frequency load shedding strategy can be used. The frequency relays installed at the non-critical loads' buses can detect the Load Shedding Frequency (LSF) and trip those loads within about 2 or 3 cycles' delay. The LSF should be set lower than the normal operational frequency of an islanded microgrid. It should be noted that although under frequency load shedding is a conventional approach that has been used in power system for decades, it cannot be directly applied in an inverter-based microgrid with conventional droop control. This is due to an inverter's frequency will not drop continuously with conventional droop control when an inverter becomes overloaded. The proposed overload mitigation controller enables the inverter's frequency to drop continuously during overload. Therefore, the under frequency load shedding can be applied in a microgrid.

Assume a grid-forming source is outputting its maximum power, its frequency drop $\Delta\omega$ after a load step is shown in equation (4). The initial frequency drop is decided by the term $(m_p + k_{ppmax})\Delta P$, and after that the frequency drops at a speed of $k_{ipmax}\Delta P$, where $\Delta P$ is the overload power. If $\Delta P$ or the proportional gain $k_{ppmax}$ is very large, the term $(m_p + k_{ppmax})\Delta P$ will be larger than $\Delta\omega_{LSF}$, which is the frequency difference between the rated frequency and LSF, as shown in Fig. 11 (a) and (b). This will cause the frequency to directly drop below LSF after the load step, thus the load will be tripped immediately after the relay's time delay, as shown in Fig. 11 (a). If $\Delta P$ or the proportional gain $k_{ppmax}$ is relatively small, the integral gain can guarantee that the frequency finally drops below the LSF, as shown in Fig. 11 (b).

$$\Delta\omega = (m_p + k_{pp\max})\Delta P + \int k_{ip\max}\Delta P dt \quad (4)$$

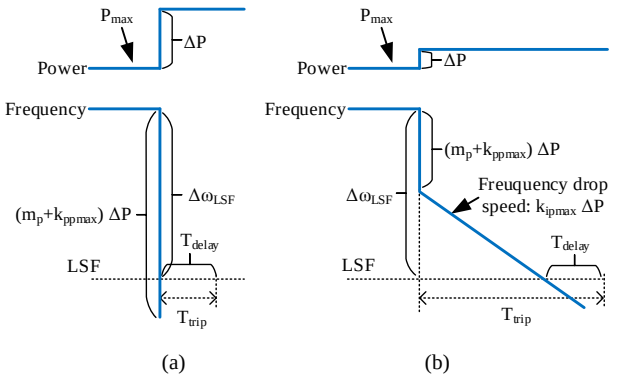


Fig. 11 Frequency drop of a grid-forming source during overload. (a) The overload power $\Delta P$ is large. (b) The overload power $\Delta P$ is small.

# IV. FIELD TEST & SIMULATION

The proposed overload mitigation controller has been verified at the CERTS/AEP test bed [2]. The CERTS/AEP microgrid test bed has conducted extensive microgrid tests over ten years. The current circuit is shown in Fig. 12. The system rated voltage is 480 V and the rated frequency is 60 Hz. A1 and A2 are commercialized inverter-based natural gas sources, and their rated capacities are 100 kW and 60 kW, respectively [21]. B1 is a 93 kW natural gas synchronous generator [22]. ESS is an inverter-based energy storage with rated 100 kW discharge and 50 kW charge capacity [23]. All the above sources are CERTS droop-controlled, grid-forming sources. There are four adjustable load banks in the microgrid, and there is a frequency relay installed at load bank 4. It should be noted that the frequency relay needs about 2 or 3 cycles' time delay to trip the load. The microgrid is connected to the grid through a static switch [3].

This article has been accepted for publication in a future issue of this journal, but has not been fully edited. Content may change prior to final publication. Citation information: DOI 10.1109/TSG.2018.2829438, IEEE Transactions on Smart Grid

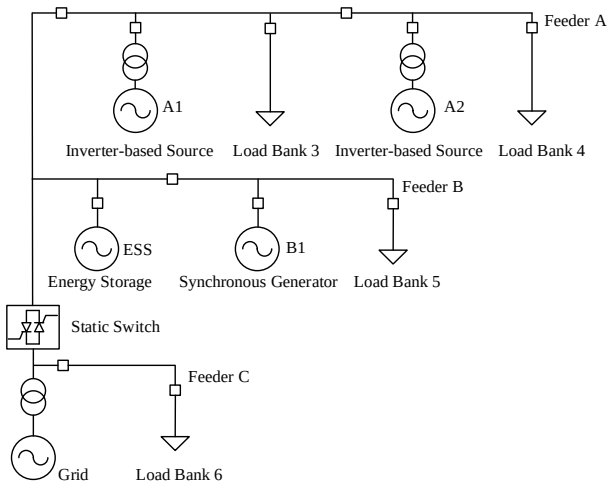


Fig. 12 One-Line Diagram of CERTS/AEP Microgrid Test Bed.

The simulation is conducted in the PSCAD/EMTDC environment. The inverter is simulated by using an average model and its controller is shown in Fig. 3. The natural gas generator model is shown in Fig. 13, it contains a synchronous machine, a droop governor, an engine, a droop AVR and an exciter. The droop governor and the droop AVR enable it to work in parallel with droop-controlled, grid-forming inverters. The details of the natural gas generator can be found in reference [22]. It should be noted that although the generator does not have an overload mitigation controller, the speed will drop continuously when the generator's electromagnetic torque $T_e$ exceeds its maximum mechanical torque $T_{max}$, this characteristic behaves similarly as an overload mitigation controller.

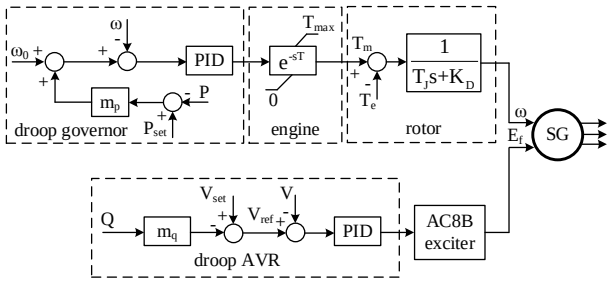


Fig. 13 Natural gas based synchronous generator model.

Three cases are tested and simulated based on CERTS/AEP test bed. Case A demonstrates the capability of the proposed overload mitigation controller to achieve overload transfer when part of the sources in a microgrid is overloaded. Case B demonstrates the capability of the proposed overload mitigation controller to activate under frequency load shedding in a purely inverter-based microgrid when all sources are overloaded. Case C demonstrates that the proposed overload mitigation controller can also activate under frequency load shedding in an inverter & generator mixed microgrid. Table 1 shows the initial conditions and the overload events of the three cases. It should be noted that case A was tested in 2008, at that time both A1 and A2 had a rated capacity of 60 kW. A1 was later replaced by a 100 kW inverter-based natural gas source in 2012. Therefore, A1 has a 100 kW rated capacity in the field tests of case B and case C.

Table 1 Microgrid initial statuses and events of three studied cases. Unit: kW

| Case | Microgrid Status | Event | A1 | A2 | B1 | ESS | Loads |
|---|---|---|---|---|---|---|---|
| A | grid-connected | islanding | 55 | 5 | off | off | 90 |
| B | islanded | trip ESS | 81 | 59 | off | 50 | 190 |
| C | islanded | trip ESS | 70 | off | 92 | 58 | 220 |

## Case A: Overload Transfer

Fig. 14 shows the simulation results of overload transfer. In this case A1 and A2 work in grid-connected mode initially with A1 outputting 55kW and A2 outputting 5kW, the total load is about 90kW, the microgrid imports about 30kW from the grid. Both A1 and A2 have a maximum 60kW capacity in this case. The microgrid goes into islanded mode at 0 s. After losing 30kW from the grid, both A1 and A2 increase about 15kW output power each to meet the extra load. This process leads to the overload of A1, so its overload mitigation controller shifts the extra load to A2 by reducing its frequency faster than the A2's frequency. The frequency difference during transient changes the phase angle between sources, so the power flow is redistributed. Finally A1 outputs its maximum generation 60kW and A2 takes the extra load. The simulation results compare well with the field test results as shown in Fig. 7. Fig. 15 shows the dynamic traces of power vs. frequency characteristic of A1 and A2, it can be seen that A1 drives the frequency down after the load step to force A2 to take the extra loads.

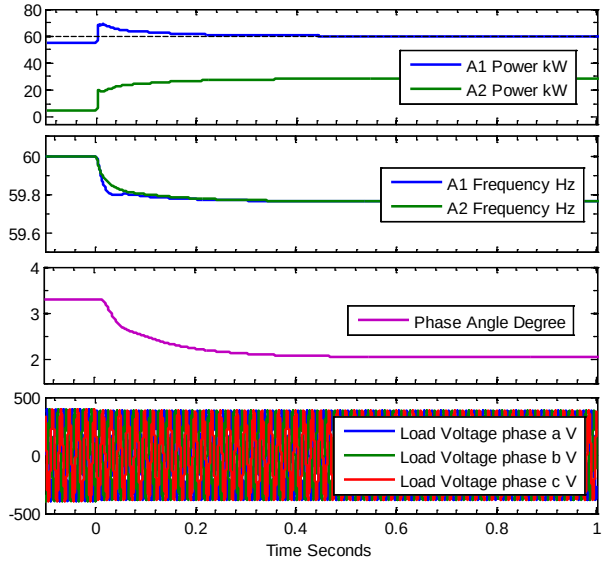


Fig. 14 Simulation of overload transfer, case A.

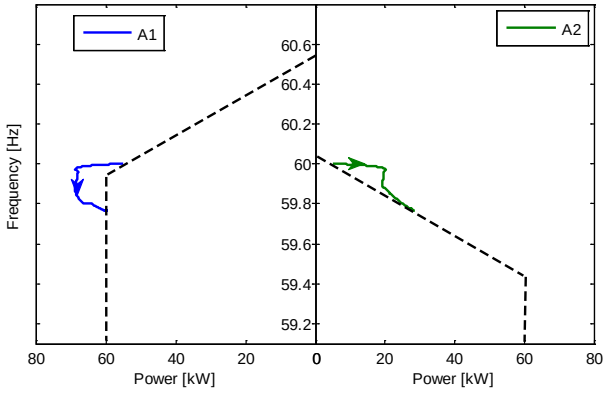


Fig. 15 Traces of P vs. f characteristics of A1 and A2, case A.

This article has been accepted for publication in a future issue of this journal, but has not been fully edited. Content may change prior to final publication. Citation information: DOI 10.1109/TSG.2018.2829438, IEEE Transactions on Smart Grid

Case B: Load Shedding, Inverter vs. Inverter

Fig. 16 (a) and Fig. 16 (b) show the AEP test and simulation results of A1 and A2 as the surviving sources after under frequency load shedding, respectively. In this case A1, A2, and ESS work together in the islanded microgrid initially with $P_{A1}$ = 81 kW, $P_{A2}$ = 59 kW, $P_{ESS}$ = 50 kW. Load bank 3, 4, 5 are online initially with $P_{LB3}$ = 95 kW, $P_{LB4}$ = 65 kW, $P_{LB5}$ = 30 kW. The total load is 190 kW. The LSF in this case is set as 59.2 Hz. At 0s the ESS is tripped as a contingency. Both A1 and A2 increase their output power to supply the load after the ESS is tripped. However, the total 190kW load exceeds the 160 kW maximum generation of A1 and A2. Both A1 and A2 become overloaded, so both overload mitigation controllers of A1 and A2 continue dropping the sources' frequencies. At about 0.47 s the LSF is reached and after about 3 cycles' delay the frequency relay trips the 65kW load bank 4, so the total load reduces from 190 kW to 125 kW and the microgrid survives. It can be seen that the simulation results compare well with field test results. Fig. 17 shows the simulation results of voltages and frequency at Load Bank 4. It can be seen that the load voltage is stiff because both A1 and A2 maintain their output voltage magnitudes approximately fixed, and the frequency is driven down by sources' overload mitigation controllers. It should be noted that the initial frequency is slightly below 60 Hz but in an acceptable range due to the setting of power set points and load level.

Fig. 18 shows the dynamic traces of power vs. frequency characteristic of A1 and A2. It can be seen that both frequencies are driven down by the overload mitigation controllers after the ESS is tripped, and after load shedding their overload mitigation controllers are deactivated so the frequencies recover to a normal range. The controller parameters of A1 in simulation are $k_{ppmax}$ = 0 rad/s, $k_{ipmax}$ = 77 rad/s$^2$, and the controller parameters of A2 in simulation are $k_{ppmax}$ = 3 rad/s, $k_{ipmax}$ = 35 rad/s$^2$. Both Fig. 17 and Fig. 18 show that the frequency slightly drops below 59.2 Hz when the load shedding is activated due to the time delay of frequency relay. However, because the controller gains are selected relatively low, the frequency only drops slightly below 59.2 Hz.

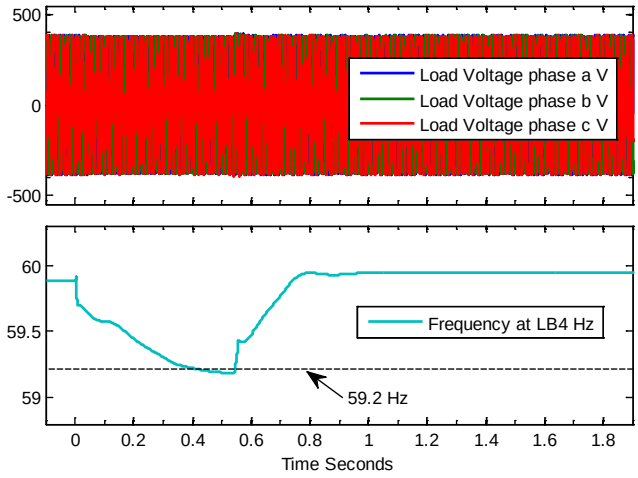


Fig. 17 Voltages and frequency at Load Bank 4, case B.

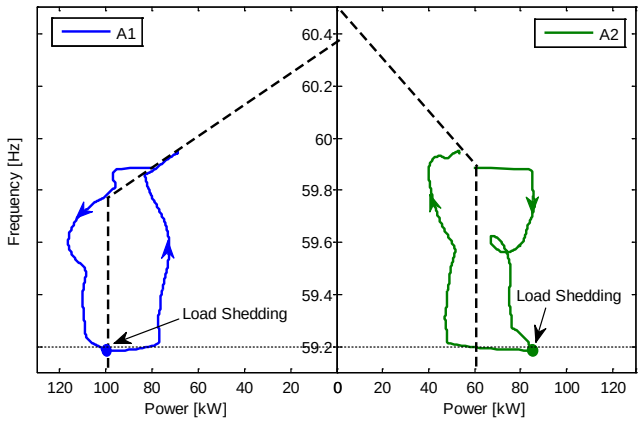


Fig. 18 Traces of P vs. f characteristic of A1 and A2, case B.

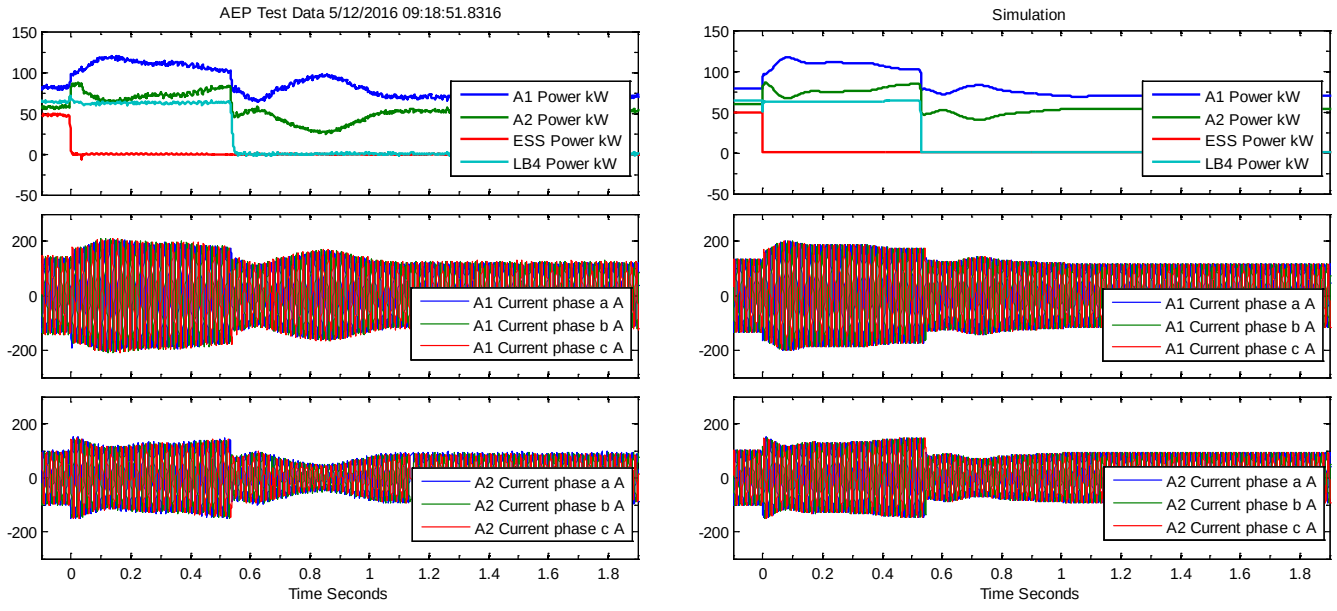


(a) AEP Field Test Data (b) Simulation

Fig. 16 Under Frequency Load Shedding, Inverter vs. Inverter, case B.

This article has been accepted for publication in a future issue of this journal, but has not been fully edited. Content may change prior to final publication. Citation information: DOI 10.1109/TSG.2018.2829438, IEEE Transactions on Smart Grid

Case C: Load Shedding, Inverter vs. Generator

Fig. 19 (a) and Fig. 19 (b) show the AEP test and simulation results of A1 and B1 as the surviving sources after under frequency load shedding, respectively. In this case A1, B1, and ESS work together in the islanded microgrid initially with $P_{A1}$=70 kW, $P_{B1}$=92 kW, $P_{ESS}$=58 kW. Load bank 3, 4, 5 are online initially with $P_{LB3}$=95 kW, $P_{LB4}$=65 kW, $P_{LB5}$=60 kW. The total load is 220 kW. The LSF in this case is set as 59 Hz. At 0s the ESS is tripped as a contingency, both A1 and B1 increase their output power to meet the load after the ESS is tripped. However, because the total 220 kW load exceeds the 193 kW maximum generations of A1 and B1, both A1 and B1 become overloaded, so the overload mitigation controller is activated to reduce the frequency. At about 0.45 s the LSF is reached and after about 3 cycles' delay the frequency relay trips the 65 kW load bank 4. It can be seen in both Fig. 19 (a) and Fig. 19 (b) that the total load reduces from 220 kW to 155 kW and the microgrid survives. The simulation results compare well with field test results. Fig. 20 shows the simulation results of voltages and frequency at Load Bank 4. It can be seen that the load voltage magnitude is robust because both the inverter and generator are grid-forming sources, and the frequency is driven down by the overload mitigation controller. The initial frequency is slightly below 60 Hz but in an acceptable range due to the setting of power set points and load level. The frequency at load bank 4 drops below 59 Hz when load shedding happens due to the time delay of frequency relay.

Fig. 21 shows the dynamic traces of power vs. frequency characteristic of A1 and B1. It can be seen that both frequencies of A1 and B1 are driven down after the ESS is tripped, and after load shedding the overload mitigation controller is deactivated so the frequencies recover to a normal range. The controller parameters of A1 in simulation are $k_{ppmax}$ = 0 rad/s, $k_{ipmax}$ = 77 rad/s$^2$. The other parameters are listed in the Appendix. It should be noted that there are about 5 Hz oscillations between A1 and B1 during transient which can be attributed to the small inertia of synchronous generator. This case shows that the proposed under frequency load shedding strategy is also effective in an inverter & generator mixed microgrid.

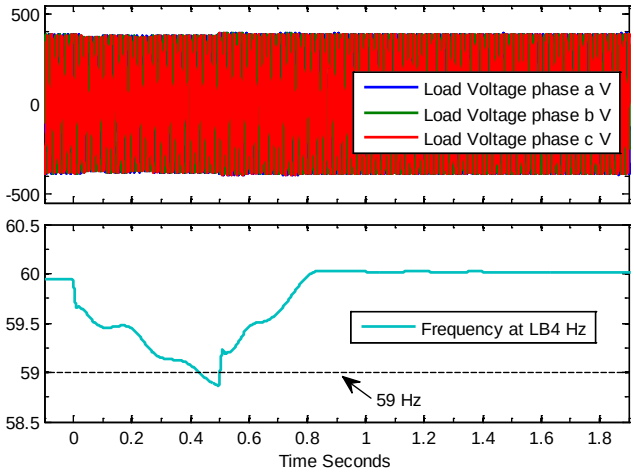


Fig. 20 Voltages and frequency at Load Bank 4, case C.

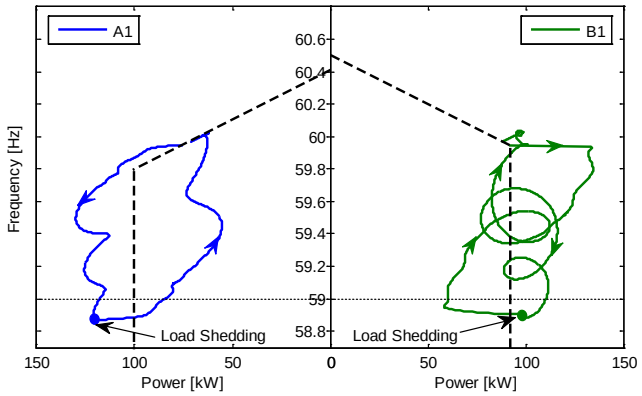


Fig. 21 Traces of P vs. f characteristic of A1 and B1, case C.

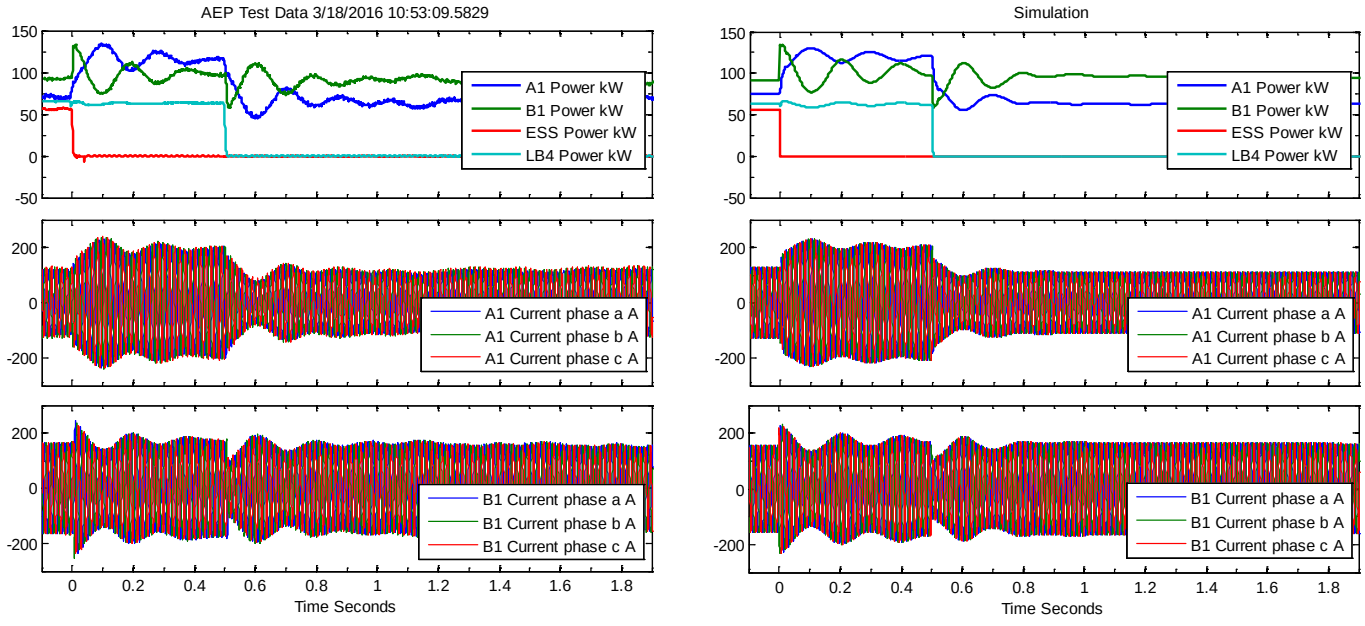


(a) AEP Field Test Data (b) Simulation

Fig. 19 Under Frequency Load Shedding, Inverter vs. Generator, case C.

This article has been accepted for publication in a future issue of this journal, but has not been fully edited. Content may change prior to final publication. Citation information: DOI 10.1109/TSG.2018.2829438, IEEE Transactions on Smart Grid

## V. SIMULATION WITH IMPROVED GAINS

In previous field tests and simulation results, the proportional gains $k_{ppmax}$ are set relatively low, so the load trip time is mainly decided by the integral gains $k_{ipmax}$. In this section both proportional gains $k_{ppmax}$ and integral gains $k_{ipmax}$ are improved to reduce the load trip time. According to Fig. 11 (a) and (b), the $k_{ppmax}$ is improved to 30 rad/s, which guarantees that the frequency can directly drop below LSF when the overload power ΔP is more than 20%. The $k_{ipmax}$ is improved to 300 rad/s$^2$ which guarantees that a 10% overload power ΔP can activate under frequency load shedding within 0.15 s.

Fig. 22 shows the simulation results of case A in Section IV with improved gains. It can be clearly seen that the frequency of A1 drops much faster than the frequency of A2 during transient which results in a fast change of phase angle, so the overload of A1 is mitigated much faster compared with Fig. 14. However, there are also significant oscillations during transient with improved gains, which is in accordance with the small signal analysis in Section III A.

Fig. 23 and Fig. 24 show the simulation results of case B and case C in Section IV with improved gains, respectively. It can be seen in Fig. 23 that the load trip time is reduced from about 0.55 s to 0.1 s for case B. This is because the controllers with improved gains reduce the frequencies much faster during overload, so the under frequency load shedding is activated earlier. Being similar with Fig. 23, Fig. 24 shows that the load trip time is reduced from 0.5 s to 0.15 s for case C. It can be seen that with improved gains the load trip times are significantly reduced for both cases. However, it should be noted that with improved gains the oscillating currents also become larger during transient. Small signal stability analysis of case B and case C can also be studied as did in Section III A, and similar stability results can be obtained. Simulation experiences indicate that the oscillating currents can reach to 4 times of the rated currents if the proportional gain $k_{ppmax}$ is increased to 60 rad/s. Therefore, the gains should be properly selected to trip the non-critical load faster and also to avoid large oscillating currents.

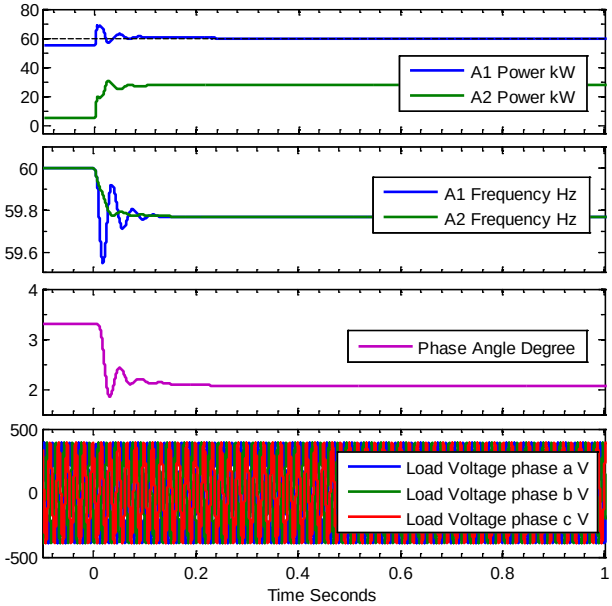


Fig. 22 Simulation of case A with improved gains.

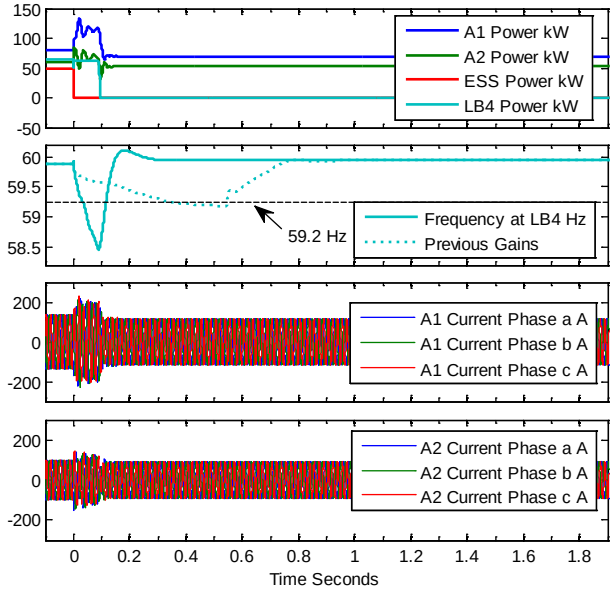


Fig. 23 Simulation of case B with improved gains.

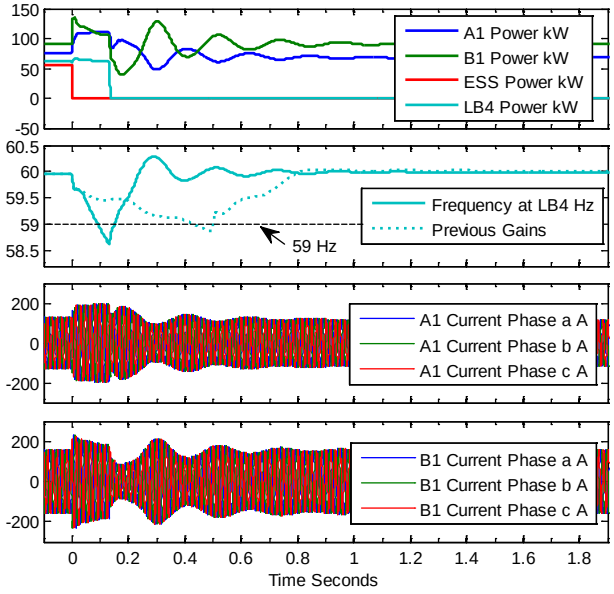


Fig. 24 Simulation of case C with improved gains.

## VI. CONCLUSION

This paper presents an overload mitigation controller that addresses the two overload issues in an autonomous microgrid. When part of the sources in a microgrid is overloaded, the controller autonomously transfers the extra load of the overloaded source to other sources by reducing its frequency rapidly. The frequency difference between sources during transient results in a change of phase angle, which redistributes the power flow. When all sources in a microgrid are overloaded, each source keeps dropping the frequency. Therefore, under frequency load shedding can be used to trip the non-critical loads resulting in the survival of microgrid. The advantages of these concepts are that communications between sources are not needed during transient, and the robust voltage control is maintained. Simulation and field test results from CERTS/AEP microgrid test site verify that this method is effective in both purely inverter-based microgrids and inverter & generator mixed microgrids.

This article has been accepted for publication in a future issue of this journal, but has not been fully edited. Content may change prior to final publication. Citation information: DOI 10.1109/TSG.2018.2829438, IEEE Transactions on Smart Grid

# VII. APPENDIX

Table 2 A1 Parameters in simulation, $V_B$=480V, $S_B$=100kW

| | | | | | |
|---|---|---|---|---|---|
| $\omega_0$ | 377 rad/s | $X_L$ | 0.15 pu | $V_{set}$ | 1 pu |
| $m_p$ | 3.77 rad/s | $m_q$ | 0.05 pu | $k_{ppmax}$ | 0 rad/s |
| $k_{ipmax}$ | 77 rad/s$^2$ | $k_{pv}$ | 0 pu | $k_{iv}$ | 5.86 pu/s |

Table 3 A2 Parameters in simulation, $V_B$=480V, $S_B$=60kW

| | | | | | |
|---|---|---|---|---|---|
| $\omega_0$ | 377 rad/s | $X_L$ | 0.12 pu | $V_{set}$ | 1 pu |
| $m_p$ | 3.77 rad/s | $m_q$ | 0.05 pu | $k_{ppmax}$ | 3 rad/s |
| $k_{ipmax}$ | 35 rad/s$^2$ | $k_{pv}$ | 0 pu | $k_{iv}$ | 5.86 pu/s |

Table 4 B1 Parameters in simulation, $V_B$=480V, $S_B$=250kW

| | | | | | |
|---|---|---|---|---|---|
| H | 0.35 s | $K_D$ | 0.000454 pu | T | 41.6 ms |
| $T_{max}$ | 0.4 pu | $X_d$ | 3 pu | $X_q$ | 2.06 pu |

## ACKNOWLEDGEMENT

This work is supported by the CERTS Microgrid program by the Office of Electricity Delivery and Energy Reliability, Transmission Reliability Program of the U.S. Dept. of Energy and administered by the Lawrence Berkeley National Laboratory.

## REFERENCES

[1] R. H. Lasseter, "MicroGrids," in *Power Engineering Society Winter Meeting, 2002. IEEE*, 2002, pp. 305-308 vol.1.
[2] R. H. Lasseter, J. H. Eto, B. Schenkman, J. Stevens, H. Vollkommer, D. Klapp, *et al.*, "CERTS Microgrid Laboratory Test Bed," *IEEE Transactions on Power Delivery*, vol. 26, pp. 325-332, 2011.
[3] R. H. Lasseter, "Smart Distribution: Coupled Microgrids," *Proceedings of the IEEE*, vol. 99, pp. 1074-1082, 2011.
[4] N. Hatziargyriou, H. Asano, R. Iravani, and C. Marnay, "Microgrids," *IEEE Power and Energy Magazine*, vol. 5, pp. 78-94, 2007.
[5] J. M. Guerrero, J. C. Vasquez, J. Matas, L. G. d. Vicuna, and M. Castilla, "Hierarchical Control of Droop-Controlled AC and DC Microgrids-A General Approach Toward Standardization," *IEEE Transactions on Industrial Electronics*, vol. 58, pp. 158-172, 2011.
[6] J. A. P. Lopes, C. L. Moreira, and A. G. Madureira, "Defining control strategies for MicroGrids islanded operation," *IEEE Transactions on Power Systems*, vol. 21, pp. 916-924, 2006.
[7] K. D. Brabandere, B. Bolsens, J. V. d. Keybus, A. Woyte, J. Driesen, and R. Belmans, "A Voltage and Frequency Droop Control Method for Parallel Inverters," *IEEE Transactions on Power Electronics*, vol. 22, pp. 1107-1115, 2007.
[8] F. Katiraei, R. Iravani, N. Hatziargyriou, and A. Dimeas, "Microgrids management," *IEEE Power and Energy Magazine*, vol. 6, pp. 54-65, 2008.
[9] N. Pogaku, M. Prodanovic, and T. C. Green, "Modeling, Analysis and Testing of Autonomous Operation of an Inverter-Based Microgrid," *IEEE Transactions on Power Electronics*, vol. 22, pp. 613-625, 2007.
[10] W. Du, Q. Jiang, M. J. Erickson, and R. H. Lasseter, "Voltage-Source Control of PV Inverter in a CERTS Microgrid," *IEEE Transactions on Power Delivery*, vol. 29, pp. 1726-1734, 2014.
[11] M. Pulcherio, A. Renjit, M. Illindala, A. Khalsa, J. Eto, D. Klapp, *et al.*, "Evaluation of Control Methods to Prevent Collapse of a Mixed Source Microgrid," *IEEE Transactions on Industry Applications*, vol. PP, pp. 1-1, 2016.
[12] A. D. Paquette and D. M. Divan, "Virtual Impedance Current Limiting for Inverters in Microgrids With Synchronous Generators," *IEEE Transactions on Industry Applications*, vol. 51, pp. 1630-1638, 2015.
[13] Z. Yao, L. Xiao, and Y. Yan, "Seamless Transfer of Single-Phase Grid-Interactive Inverters Between Grid-Connected and Stand-Alone Modes," *IEEE Transactions on Power Electronics*, vol. 25, pp. 1597-1603, 2010.
[14] D. S. Ochs, B. Mirafzal, and P. Sotoodeh, "A Method of Seamless Transitions Between Grid-Tied and Stand-Alone Modes of Operation for Utility-Interactive Three-Phase Inverters," *IEEE Transactions on Industry Applications*, vol. 50, pp. 1934-1941, 2014.
[15] R. Shi, X. Zhang, H. Xu, F. Liu, W. Li, F. Mao, *et al.*, "A method for microgrid connected fuel cell inverters seamless transitions between voltage source and current source modes," in *2015 9th International Conference on Power Electronics and ECCE Asia (ICPE-ECCE Asia)*, 2015, pp. 2718-2723.
[16] X. Lu, J. Wang, J. Guerrero, and D. Zhao, "Virtual Impedance Based Fault Current Limiters for Inverter Dominated AC Microgrids," *IEEE Transactions on Smart Grid*, vol. PP, pp. 1-1, 2016.
[17] J. He and Y. W. Li, "Analysis, Design, and Implementation of Virtual Impedance for Power Electronics Interfaced Distributed Generation," *IEEE Transactions on Industry Applications*, vol. 47, pp. 2525-2538, 2011.
[18] P. Piagi and R. H. Lasseter, "Autonomous control of microgrids," in *2006 IEEE Power Engineering Society General Meeting*, 2006, p. 8 pp.
[19] M. J. Erickson, "Improved power control of inverter sources in mixed-source microgrids," Ph.D. dissertation, Dept. Elect. Comput. Eng., Univ. Wisconsin-Madison, Madison, WI, USA, 2013.
[20] W. Du and R. H. Lasseter, "Overload mitigation control of droop-controlled grid-forming sources in a microgrid," in *2017 IEEE Power & Energy Society General Meeting*, 2017, pp. 1-5.
[21] *InVerde*. Available: https://www.tecogen.com/chp-cogeneration/inverde
[22] A. A. Renjit, M. S. Illindala, R. H. Lasseter, M. J. Erickson, and D. Klapp, "Modeling and control of a natural gas generator set in the CERTS microgrid," in *2013 IEEE Energy Conversion Congress and Exposition*, 2013, pp. 1640-1646.
[23] A. S. Khalsa and S. Baktiono. *CERTS Microgrid Test Bed Battery Energy Storage System Report: Phase 1*. Available: https://certs.lbl.gov/publications/certs-microgrid-test-bed-battery

**Wei Du** received the Ph.D. in Electrical Engineering from Tsinghua University, Beijing, China in 2014. He was a Visiting Student with the University of Wisconsin-Madison from 2012 to 2013. He worked as a Research Engineer in the key Real Time Digital Simulation (RTDS) lab of power system in China Southern Power Grid Company from 2014 to 2016. He worked as a Research Associate at the University of Wisconsin-Madison from 2016 to 2018. He is currently a Senior Research Engineer at the Pacific Northwest National Laboratory. His research interests include microgrids, distribution system resiliency, control of distributed energy resources, hardware-in-the-loop simulation, power system dynamic modeling and analysis, and control of HVDC and FACTS. He received the Best of the Best Conference Paper Award in the IEEE PES General Meeting in 2017. He received the Best Reviewer Awards of IEEE Transactions on Smart Grid in 2016 and 2017.

**Robert H. Lasseter** (M'74, SM'89, F'92, LF'07) received the Ph.D. in Physics from the University of Pennsylvania, Philadelphia in 1971. He was a Consulting Engineer at General Electric Co. until he joined the University of Wisconsin-Madison in 1980. Dr. Lasseter is internationally recognized as one of the earliest and most influential pioneers in the microgrid field. His professional career during the past 40 years has been dedicated to applying power electronics to utility systems. He is the technical lead for the Consortium for Electrical Reliability Technology Solutions' (CERTS) Microgrid Project. CERTS's microgrid architecture is widely implemented and recognized for its plug-and-play flexibility. Prof. Lasseter is past chair of the IEEE Working Group on Distributed Resources and an IEEE Distinguished Lecturer in distributed resources.

**Amrit Khalsa** (M'91) received the B.S. and M.S. degrees in electrical engineering from The Ohio State University, Columbus, Ohio, USA in 1984 and 2011 respectively. From 1984 to 1987, he was a Teaching Assistant with the Electrical Engineering Department, the Ohio State University. Since 1988, he has held various engineering and management positions with American Electric Power (AEP), Columbus, Ohio, in the areas of System Protection & Control, Underground Systems Engineering, Distribution System Planning, Geospatial Information Systems, and Advanced Technology Testing. He is currently a Staff Engineer at AEP's Dolan Technology Center. He is an author/coauthor of papers in areas including microgrids and electric transportation. His research interests include microgrids, distributed energy resources, and smart grid technology from the distribution system down to the customer. Mr. Khalsa is a registered Professional Engineer in the State of Ohio. He is the recipient of an EPRI Technology Transfer Award in 2012 for contributions to developing ANSI Standard CEA-2045, a modular communication interface for demand response.